

---

This is an electronic reprint of the original article.  
This reprint may differ from the original in pagination and typographic detail.

Jussila, Henri; Kivisaari, Pyry; Lemettinen, Jori; Tanaka, Tooru; Sopanen, Markku  
**Two-Photon Absorption in GaAs<sub>1-x</sub>PyN<sub>x</sub> Intermediate-Band Solar Cells**

*Published in:*  
Physical Review Applied

*DOI:*  
[10.1103/PhysRevApplied.3.054007](https://doi.org/10.1103/PhysRevApplied.3.054007)

Published: 01/01/2015

*Document Version*  
Publisher's PDF, also known as Version of record

*Please cite the original version:*  
Jussila, H., Kivisaari, P., Lemettinen, J., Tanaka, T., & Sopanen, M. (2015). Two-Photon Absorption in GaAs<sub>1-x</sub>PyN<sub>x</sub> Intermediate-Band Solar Cells. *Physical Review Applied*, 3(5), 1-9. Article 054007.  
<https://doi.org/10.1103/PhysRevApplied.3.054007>

---

This material is protected by copyright and other intellectual property rights, and duplication or sale of all or part of any of the repository collections is not permitted, except that material may be duplicated by you for your research use or educational purposes in electronic or print form. You must obtain permission for any other use. Electronic or print copies may not be offered, whether for sale or otherwise to anyone who is not an authorised user.

## Two-Photon Absorption in $\text{GaAs}_{1-x-y}\text{P}_y\text{N}_x$ Intermediate-Band Solar Cells

H. Jussila,<sup>1,\*</sup> P. Kivisaari,<sup>2</sup> J. Lemettinen,<sup>1</sup> T. Tanaka,<sup>3</sup> and M. Sopanen<sup>1</sup>

<sup>1</sup>*Department of Micro and Nanosciences, Aalto University, P.O. Box 13500, FI-00076 Aalto, Finland*

<sup>2</sup>*Department of Biomedical Engineering and Computational Science, Aalto University, P.O. Box 12200, FI-00076 Aalto, Finland*

<sup>3</sup>*Department of Electrical and Electronic Engineering, Saga University, 1 Honjo, Saga 840-8502, Japan and PRESTO, Japan Science and Technology Agency (JST), Kawaguchi, Saitama 332-0012, Japan*  
(Received 21 October 2014; revised manuscript received 20 March 2015; published 14 May 2015)

We demonstrate that a two-photon absorption process occurs in a  $\text{GaAs}_{1-x-y}\text{P}_y\text{N}_x$ -based solar cell in which a  $\text{GaAs}_{0.31}\text{P}_{0.68}\text{N}_{0.01}$  layer is implemented in the heterostructure and the  $E_-$  energy band is isolated using an AIP blocking layer. The observed transition energies in external quantum-efficiency spectra correspond to the  $E_-$  and  $E_+$  energy bands of the  $\text{GaAs}_{0.31}\text{P}_{0.68}\text{N}_{0.01}$  alloy and agree with the photoreflectance results. With photon energy smaller than the transition between the valence band and the  $E_-$  band, the absorption of IR light increases the quantum efficiency by over 10% at room temperature and significantly more at lower temperatures due to the suppression in the thermionic emission. The effects of two-photon absorption on the  $I$ - $V$  characteristics and output power of the fabricated  $\text{GaAs}_{1-x-y}\text{P}_y\text{N}_x$  solar cell are studied by current transport simulations. We show how doping of the intermediate band and current transport between the intermediate band and surrounding regions affect the operation of  $\text{GaAs}_{1-x-y}\text{P}_y\text{N}_x$  solar cells. Simulations under 1 Sun illumination result in an enhancement of 6% in the power density compared to a corresponding reference single-junction cell.

DOI: 10.1103/PhysRevApplied.3.054007

### I. INTRODUCTION

An intermediate-band solar cell (IBSC) is a semiconductor device capable of converting solar radiation into electricity with a conversion efficiency larger than the Shockley-Quisser limit [1,2]. The operation of an IBSC is based on the peculiar energy-band structure of certain semiconductor alloys which can be implemented in the cell design such that an intermediate energy band (IB) exists between the conduction band and the valence band of a typical two-band solar cell. As a result, an IBSC is capable of absorbing a large portion of the solar spectrum with high efficiency. Previous IBSC devices typically use two different concepts. The coupling between the energy states of quantum dots embedded inside the active region of a single-junction solar cell can induce an intermediate energy band. For instance, this IB is shown to exist in various quantum structures such as InAs/GaAs QDs [3,4], InAs quantum dots (QDs) embedded inside  $\text{GaAs}/\text{Al}_x\text{Ga}_{1-x}\text{As}$  quantum wells (QWs) [5], and GaSb/GaAs QDs [6]. On the other hand, maybe a more promising approach is the utilization of highly mismatched semiconductor alloys. Examples of IBSC work conducted on highly mismatched semiconductor alloys comprise dilute nitride semiconductors [7–9] and oxygen-doped ZnTe [10]. In these alloys, the incorporation of a small amount of nitrogen or oxygen splits the conduction band of the material into two energy

bands, i.e.,  $E_+$  and  $E_-$ , which then operate as the conduction band and the intermediate band of the device, respectively.

One key requirement for the operation of a dilute nitride-based IBSC is that the quasi-Fermi-level of the  $E_-$  energy band, which is typically the conduction band of the dilute nitride material, is different from the quasi-Fermi-level of the conduction band of the device [11]. This condition enables the open-circuit voltage of the device to be defined by the difference between the quasi-Fermi-level of the  $E_+$  energy band and the quasi-Fermi-level of the valence band. An important consequence for the isolation of the  $E_-$  band is that two-photon excitation can create excess photocurrent. Lopez *et al.* show that, by using  $\text{GaAs}_{1-x}\text{N}_x/\text{Al}_x\text{Ga}_{1-x}\text{As}$  heterostructure, the energy-band lineup can be engineered so that the energy-band discontinuity at the interface isolates the  $E_-$  energy band from the conduction band of the device and the open-circuit voltage of the device increases [8]. Two-photon excitation also increases the photocurrent of such a device [9]. In those works, it is possible to realize the energy-band discontinuity at the interface because of the large differences in the electron affinities of  $\text{Al}_x\text{Ga}_{1-x}\text{As}$  (3.63 eV) and  $\text{GaAs}_{1-x}\text{N}_x$  ( $\sim 4.1$  eV).

$\text{GaAs}_{1-x-y}\text{P}_y\text{N}_x$  is another semiconductor alloy which draws a lot of attention because of similar material properties [7,12]. The advantages of  $\text{GaAs}_{1-x-y}\text{P}_y\text{N}_x$  in comparison to  $\text{GaAs}_{1-x}\text{N}_x$ , however, lie in its quaternary nature, which provides more freedom to engineer more suitable

\*henri.jussila@aalto.fi

absorption properties of the device. For instance, Kudrawiec *et al.* point out that the  $E_-$  energy band is more narrow in  $\text{GaAs}_{1-y-x}\text{P}_y\text{N}_x$  than in  $\text{GaAs}_{1-x}\text{N}_x$  because the energy band is extended from the N states when P content is larger than  $y > 0.4$ . Therefore, a larger separation between the  $E_+$  and  $E_-$  energy bands is predicted, which possibly enhances the operation of the IBSC device [12]. The other advantages of  $\text{GaAs}_{1-x-y}\text{P}_y\text{N}_x$  include that it can be both  $p$ -type and  $n$ -type doped and the material composition can be selected so that the transition energies between the valence band and the  $E_+$  and  $E_-$  energy bands provide an optimum spectral response. However, the isolation of the  $E_-$  band has not yet been demonstrated and the two-photon absorption processes have not been observed in  $\text{GaAs}_{1-x-y}\text{P}_y\text{N}_x$  alloys with P content larger than  $y > 0$ . In this work, we demonstrate experimentally that two-photon absorption can occur in a  $\text{GaAs}_{1-x-y}\text{P}_y\text{N}_x$  solar cell. The experimental results are measured from a solar cell in which a  $\text{GaAs}_{0.31}\text{P}_{0.68}\text{N}_{0.01}$  layer is implemented in the heterostructure and an AIP layer is used for intermediate-band blocking. Device simulations are used to show the potential advantages of two-photon absorption on the  $I$ - $V$  characteristics and output power of the fabricated  $\text{GaAs}_{1-x-y}\text{P}_y\text{N}_x$  solar cell.

## II. EXPERIMENT

Experimental results are measured from solar-cell devices grown by metal-organic vapor-phase epitaxy. The precursors are trimethylgallium, tertiarybutylarsine, trimethylaluminum, tertiarybutylphosphine, and dimethylhydrazine for gallium, arsenic, aluminum, phosphorus, and nitrogen, respectively. In addition, silane and diethylzinc are used as silicon and zinc sources for  $n$ -type and  $p$ -type doping, respectively. The sample structure labeled SC1 is shown schematically in Fig. 1. In this device, a 600-nm-thick layer of  $n$ -doped  $\text{GaAs}_{0.31}\text{P}_{0.68}\text{N}_{0.01}$  is sandwiched between the 500-nm-thick  $p$ -type GaP emitter layer and the  $n$ -type GaP substrate. The growth conditions and determination of the  $\text{GaAs}_{0.31}\text{P}_{0.68}\text{N}_{0.01}$  in layer's composition are reported elsewhere [13]. An AIP layer with a thickness of 40 nm is grown between the  $n$ -doped light-absorbing  $\text{GaAs}_{0.31}\text{P}_{0.68}\text{N}_{0.01}$  layer and the  $n$ -type GaP substrate for intermediate-band blocking. In addition, two reference samples are grown without the AIP blocking layer and these are referred to as samples R1 and R2. In sample R1, the  $n$ -doped  $\text{GaAs}_{0.31}\text{P}_{0.68}\text{N}_{0.01}$  layer is grown under the same conditions as in sample SC1. In sample R2, the  $\text{GaAs}_{0.31}\text{P}_{0.68}\text{N}_{0.01}$  layer is grown without  $n$ -type dopant flow. The differences between the samples are listed in Table I. The doping concentration of the  $p$ -type emitter layer is measured by Hall measurement to be  $8 \times 10^{18}/\text{cm}^3$ . The doping concentration of the  $n$ -type GaP substrate is given by the substrate manufacturer to be between  $2 \times 10^{17}/\text{cm}^3$  and  $2 \times 10^{18}/\text{cm}^3$ . Back-side

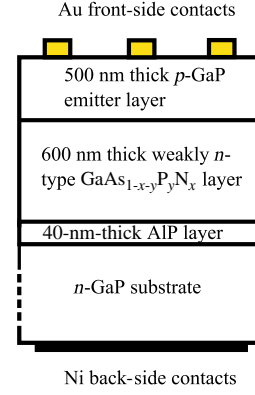


FIG. 1. Schematics of the structure of sample SC1. The structure of samples R1 and R2 is otherwise similar except the 40 nm thick AIP layer is missing.

and front-side Ohmic contacts are fabricated from nickel and gold, respectively, and annealed for 10 min at 500 °C in  $\text{N}_2$  atmosphere.

The external quantum efficiency (EQE) of the solar-cell devices is measured to examine the absorption properties of the samples using a 250 W tungsten halogen lamp and a grating monochromator. The light from the tungsten halogen lamp is modulated with a chopper allowing the photovoltaic (PV) response to be extracted from the monochromator output using a lock-in amplifier. In addition to EQE, in order to prove the photocurrent induced by two-step photon absorption via an intermediate band, the EQE of the solar-cell devices is recorded with and without an infrared light illumination as a bias light at room temperature. A 500-W Xe lamp is used as the IR light source with a sharp cutoff filter which passes photons with the wavelength longer than 1000 nm (or the photon energy below 1.24 eV). With the IR illumination, the excess electrons in the IB can be excited to the conduction band, producing an additional photocurrent. The EQE is recorded with and without the IR illumination, and the percentage increase in EQE with IR light illumination is calculated as  $\Delta Q = (Q_{\text{IR,on}} - Q_{\text{IR,off}})/Q_{\text{IR,off}}$ , where  $Q$  is the quantum efficiency.

One-dimensional current transport simulations similar to Ref. [14] are performed to further interpret the experimental results and to understand the device's operation. The self-consistent model included Poisson's equation for solving the band diagrams and drift-diffusion equations for solving

TABLE I. Sample information.

Sample	$\text{GaAs}_{0.31}\text{P}_{0.68}\text{N}_{0.01}$	AIP layer
SC1	$n$ -type	yes
R1	$n$ -type	no
R2	intrinsic	no

electron and hole transport. Drift-diffusion simulation is also performed for the  $E_-$  band but, as in most drift-diffusion simulations of intermediate-band solar cells (see, e.g., Refs. [14–16]), electron current through the interfaces of the  $E_-$  band is set to zero (except for one illustrative case, explained in more detail in Sec. III). Absorption rates are calculated based on the band-edge energies, the dispersion relation of the bands given by the band anticrossing model, and the radiation spectrum of the Sun. Radiative recombination is calculated as  $Bn_i^2\{\exp[-e\Delta E_F/(k_B T)] - 1\}$ , where  $B$  is the radiative recombination coefficient,  $n_i$  is the intrinsic carrier concentration,  $e$  is the elementary charge,  $\Delta E_F$  is the difference between the quasi-Fermi-levels of the bands that produce the recombination,  $k_B$  is Boltzmann's constant, and  $T$  is the temperature. The model is also very similar to the model used in Ref. [17] for III-nitride LEDs. The parameters required for simulations are obtained from Refs. [12,18–20].

### III. RESULTS AND DISCUSSION

#### A. Experimental proof of two-photon absorption signal

In order to gather information from the energy-band structure of the  $\text{GaAs}_{0.31}\text{P}_{0.68}\text{N}_{0.01}$  layer, photoreflectance measurements are performed on a 20-nm-thick  $\text{GaAs}_{0.31}\text{P}_{0.68}\text{N}_{0.01}$  layer grown on an  $n$ -GaP substrate with the same growth parameters as the 600-nm-thick  $\text{GaAs}_{0.31}\text{P}_{0.68}\text{N}_{0.01}$  layers. Figure 2 shows the measured photoreflectance spectrum, in addition to the external-quantum-efficiency spectra of all the samples mentioned in Table I. The photoreflectance spectrum shows transitions from the split conduction band of the  $\text{GaAs}_{0.31}\text{P}_{0.68}\text{N}_{0.01}$  layer at 1.94 eV and 2.44 eV, in addition to the transition from the GaP substrate at 2.78 eV. The splitting of the conduction band in  $E_+$  and  $E_-$  energy bands is reported to occur due to an anticrossing interaction between the nitrogen-induced energy states and the  $\text{GaAs}_{1-x}\text{P}_x$  host alloy [7,21]. The location of these  $E_+$  and  $E_-$  transitions agrees relatively well with the shape of the external-quantum-efficiency spectrum, and thus, the features visible in the EQE spectrum are due to the split conduction band of the  $\text{GaAs}_{0.31}\text{P}_{0.68}\text{N}_{0.01}$  layer. In addition, it can be observed that the shape of the EQE spectrum and especially the relative magnitude of the  $E_-$  transition are influenced by the doping concentration of the  $\text{GaAs}_{0.31}\text{P}_{0.68}\text{N}_{0.01}$  layer and also by the existence of the AIP IB blocking layer. Note that the composition of the  $\text{GaAs}_{0.31}\text{P}_{0.68}\text{N}_{0.01}$  layer may vary slightly between the different growth runs, possibly explaining the different locations ( $\pm 50$  meV) for the peaks visible in EQE spectrum. However, the composition variations cannot explain the changes in the shape of the spectrum. The spectral shape is most likely influenced by the different internal electric field and the energy-band

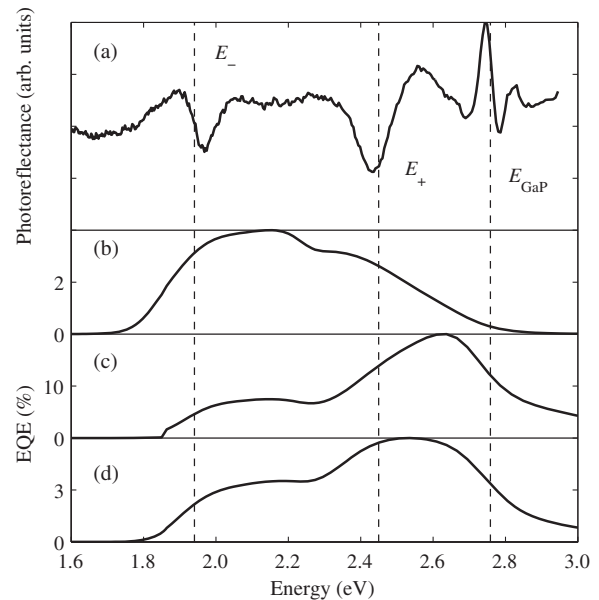


FIG. 2. Comparison between (a) the photoreflectance spectrum of a 20-nm-thick  $\text{GaAs}_{0.31}\text{P}_{0.68}\text{N}_{0.01}$  layer and the EQE spectrum of samples (b) R2, (c) R1, and (d) SC1.

lineups over the  $\text{GaAs}_{0.31}\text{P}_{0.68}\text{N}_{0.01}/n$ -GaP interface caused by the different doping concentrations of the samples and the presence of an AIP IB blocking layer.

The shape of the EQE spectrum of samples R1 and SC1 differs from that of sample R2, which shows the largest EQE signal for photons with the energy corresponding to the  $E_-$  energy band. This is typical behavior for single-junction semiconductor solar cells in which the EQE maximum is slightly above the band gap of the material. However, for samples R1 and SC1, the location of the EQE spectrum maximum is roughly at 2.6 eV, which is about 100 meV larger than the transition energy from the valence band to the  $E_+$  band. Thus, the shape of EQE spectrum suggests that the band-gap value is defined by the  $E_+$  energy band instead of the  $E_-$  band and that the  $E_-$  energy band could at least be partially isolated from the conduction band of the  $n$ -type GaP substrate. However, the fact that the EQE is larger than zero for the photons with energy corresponding to the  $E_-$  transition could indicate that the energy-band discontinuity is not enough to completely isolate the  $E_-$  energy band from the conduction band of the device.

The external quantum efficiency of all the samples is rather low (typically below 10% and maximum 20%). This is not surprising and can at least be partially attributed to the lack of antireflection coatings and to the poor material quality of the grown dilute nitride layers (dilute nitrides typically possess high densities of nitrogen-related point defects [22]). These point defects decrease the lifetime of photoexcited charge carriers, and therefore, their presence is likely to hinder the current conduction. Similar issues are

discussed in the literature [9,23]. In addition, it is worth noting that the presence of an AIP layer is likely to have an effect on current transport and thereby also on the magnitude of EQE. Furthermore, the grown samples are highly lattice mismatched, causing the lattice strain to relax via formation of a misfit dislocation network. The lattice mismatch between the  $\text{GaAs}_{0.31}\text{P}_{0.68}\text{N}_{0.01}$  and the growth substrate could be reduced by fabricating the structure on graded  $\text{GaAs}_{1-x}\text{P}_x$  buffer layers [24].

To gather direct evidence from two-photon excitation, a  $\Delta\text{QE}$  spectrum is measured from all the samples (shown in Fig. 3). Note that Fig. 3 plots the percentage increase in quantum efficiency with IR light illuminating the sample. The wavelength of the IR light corresponds to energies smaller than 1.24 eV, thus being capable of exciting charge carriers from the  $E_-$  band to the  $E_+$  band. However, the photon energy is not enough to excite charge carriers from the valence band to the  $E_-$  band, and therefore, is itself incapable of creating any photocurrent signal, as also observed in Fig. 2. As a result, if a signal larger than zero is observed, this observation implies that the QE increases with the absorption of IR light, thus providing evidence of two-photon absorption-induced photocurrent.

It can be observed that the absorption of IR light increases the QE of samples R1 and SC1. In these samples, the  $\Delta\text{QE}$  spectra show increases in QE in three regions, i.e., (1) a peak near the photon energy corresponding to the  $E_-$  energy band, (2) a plateau between the  $E_-$  and  $E_+$  energy bands, and (3) an increase in the  $\Delta\text{QE}$  signal with increasing photon energy if the photon energy is larger than the  $E_+$  energy band. The shape of the spectrum can be explained by the processes that a charge carrier experiences and that spectrum shape is explained in Sec. III B, with the calculated energy-band diagram of the devices. However,

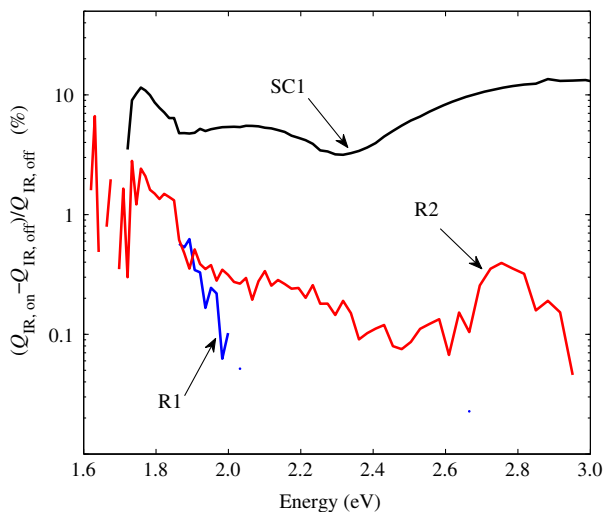


FIG. 3. Increase in quantum efficiency with IR light illuminating the sample.

to gather direct evidence from the importance of the AIP blocking layer, it is important to study the relative increase in QE with IR light. The magnitude of the QE increase is at least one decade smaller for sample R1 than for SC1, which can show an increase in QE up to 15%. This behavior suggests that  $n$ -type doping in the  $\text{GaAs}_{0.31}\text{P}_{0.68}\text{N}_{0.01}$  layer and the use of the AIP layer give rise to two-photon absorption-induced photocurrent. On the other hand, for sample R2, the absorption of IR light is not creating any significant difference in the QE spectrum, implying that the photoexcited charge carriers escape from the  $E_-$  band directly outside the  $pn$  junction and, therefore, are not required to be first excited to the  $E_+$  band before being able to create any photocurrent. As a result, two-photon absorption in sample R2 is not inducing any excess photocurrent, and thus, it seems that the inclusion of an intermediate-band blocking layer and  $n$ -type doping is required for IBSC operation.

### B. Band diagram of the fabricated $\text{GaAs}_{0.31}\text{P}_{0.68}\text{N}_{0.01}$ solar cells

To explain the experimental results, the energy-band diagram of each sample is simulated and is shown in Fig. 4. We choose to show the results in the short-circuit condition without illumination because, as the illumination flux used in EQE measurement is quite small, that is the condition best replicating the measurements. It can be observed that the presence of an AIP blocking layer creates a potential barrier between the  $E_-$  energy band and the conduction band of the  $n$ -type GaP substrate. The magnitude of the potential barrier is obtained from the electron affinities of the materials, using the Anderson rule, and is 0.3 eV. In the case of samples R1 and R2, there is no AIP blocking layer

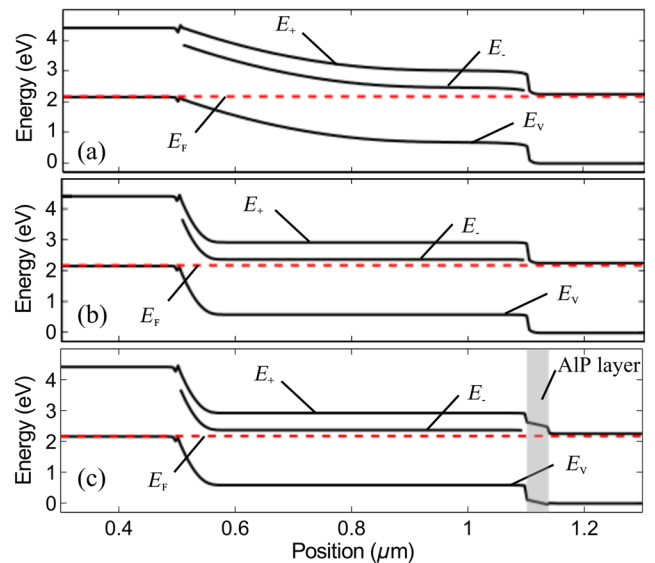


FIG. 4. Simulated band diagrams at short-circuit condition for samples (a) R2, (b) R1, and (c) SC1.

and the potential barrier is only determined by the band offset between  $E_-$  and GaP. In addition, we note that the effect of the potential barrier could be increased by selecting a  $\text{GaAs}_{1-x-y}\text{P}_y\text{N}_x$  alloy with larger As or N content or by simply growing a thicker AIP layer.

The energy-band lineup engineering using small electron-affinity material is a concept similar to that used by Lopez *et al.* in the fabrication of an IBSC from  $\text{GaAs}_{1-x}\text{N}_x$ . In that work, the small electron-affinity of  $\text{Al}_x\text{Ga}_{1-x}\text{As}$  is used to perturbate the energy bands of the large-electron-affinity  $\text{GaAs}_{1-x}\text{N}_x$ , so that the  $E_-$  energy band is disconnected from the conduction band of the  $n$ -type substrate [8]. Thus, the advantage that is gained by designing the structure similarly (but this time by using an AIP layer) is that, in order for the charge carriers in the  $E_-$  band to move towards the  $n$ -type GaP substrate, they have to bypass the 40-nm-thick 0.3-eV-high potential barrier. Note that there are different mechanisms for charge-carrier transport through potential barriers—in this case the most important being thermionic emission of carriers. Tunneling through the 40-nm-thick AIP barrier also occurs but can be assumed to be relatively weak and the effect can be further reduced by growing a thicker AIP barrier layer.

The difference in the absolute magnitude of the EQE between samples SC1 and R1 can partially be explained by the potential barrier created by the AIP layer, which hinders the movement of photoexcited charge carriers. However, if electron current between the  $E_-$  band of  $\text{GaAs}_{0.31}\text{P}_{0.68}\text{N}_{0.01}$  and the  $n$ -type GaP is blocked, then the photoexcitation of charge carriers from the  $E_-$  band to the  $E_+$  energy band provides an alternative means to overcome the diffusion barrier. This phenomenon enables the subbandgap photons to contribute to the photocurrent magnitude via two-photon absorption processes and is observed in Fig. 3. Moreover, a similar effect can cause the increase of the  $\Delta\text{QE}$  signal at energies larger than the  $E_+$  band, which is also observed in Fig. 3. In this case, due to the short lifetime of the photoexcited charge carriers in the  $E_+$  energy band, they are likely to relax to the  $E_-$  energy band before exiting the  $pn$  junction. After relaxation, these charge carriers have to bypass the potential barrier created by the AIP layer. In this case, the absorption of IR light can re-excite the relaxed charge carriers back to the  $E_+$  band, and therefore, increase the QE. A similar explanation in Ref. [9] proposes a large  $\Delta\text{QE}$  signal at energies larger than the  $E_+$  energy band inside the examined  $\text{GaAs}_{1-x}\text{N}_x$ -based IBSCs. On the other hand, if no IB blocking layer exists, then the charge carriers are predicted to escape more easily from the  $E_-$  band directly to the  $n$ -type GaP substrate before being photoexcited to the  $E_+$  energy band. In this case, two-photon absorption is not making any significant difference for the magnitude of the photocurrent, thereby agreeing with the experimental results. Finally, we note that the small difference between the  $\Delta\text{QE}$  results of reference

samples R1 and R2 may relate to different doping concentrations of the  $\text{GaAs}_{0.31}\text{P}_{0.68}\text{N}_{0.01}$  layer, which create different electric fields over the  $\text{GaAs}_{0.31}\text{P}_{0.68}\text{N}_{0.01}$ -GaP junction.

### C. Thermionic emission through the AIP layer

To gather more evidence from the movement of charge carriers through the potential barrier created by the AIP layer, we measure the EQE and  $\Delta\text{QE}$  of sample SC1 as a function of temperature. The results obtained from these measurements are shown in Fig. 5. It can be observed that the EQE signal decreases everywhere and  $\Delta\text{QE}$  increases with decreasing temperature in the energy range corresponding to the transition between the valence band and the  $E_-$  band. We note that this trend applies when the temperature is larger than 100 K (for clarity reasons, the temperature-dependent  $\Delta\text{QE}$  spectra are not shown for every temperature). In addition, the ratio between the integrated EQE of the energy range corresponding to the  $E_-$  and the  $E_+$  energy transition [i.e., the ratio between the unshaded and the shaded regions of Fig. 5(a)] decreases with the decreasing temperature and saturates below 150 K.

Temperature affects the behavior of the charge carriers at least via the following effects: (1) the lifetime of the charge carriers increases and (2) the thermionic emission rate over the AIP layer decreases with decreasing temperature. For instance, the nonradiative charge-carrier lifetime in silicon depends on the temperature with  $\tau(T) = \tau_{300\text{ K}}(T_{300\text{ K}}/T)^{3/2}$  [25]. If we use the same relation for  $\text{GaAs}_{0.31}\text{P}_{0.68}\text{N}_{0.01}$ , we can estimate that the lifetime of charge carriers increases about by a factor of 2 when the temperature decreases from 300 K to 200 K. On the other hand, the thermionic emission rate  $r$  is dependent on the temperature with  $r \propto T^2 \exp(\Delta E/k_B T)$ , in which  $\Delta E = 0.3$  eV is the size of the energy barrier,  $k_B$  is the Boltzmann constant, and  $T$  the temperature [plotted in the inset of Fig. 5(b)]. Thus, it can be estimated that the thermal emission rate decreases by a factor of 750 when the temperature decreases from 300 K to 200 K. And, (3) the deionization of dopant atoms with decreasing temperature increases the resistivity of the cell but can be estimated to occur effectively only below 100 K.

The results shown in Fig. 5 are affected the strongest by the decrease of thermal emission rate through the AIP barrier. The reduction in the thermal emission explains the drop in EQE and also the increase in  $\Delta\text{QE}$  with the decrease in temperature in the energy range corresponding to the  $E_-$  energy transition. Due to the suppression of thermionic emission, photocurrent created by electrons flowing from the  $E_-$  band to the  $n$ -GaP decreases significantly as the temperature decreases. Therefore, excitation by IR light has an increasing effect on the EQE at the energy corresponding to the  $E_-$  transition as the temperature decreases and

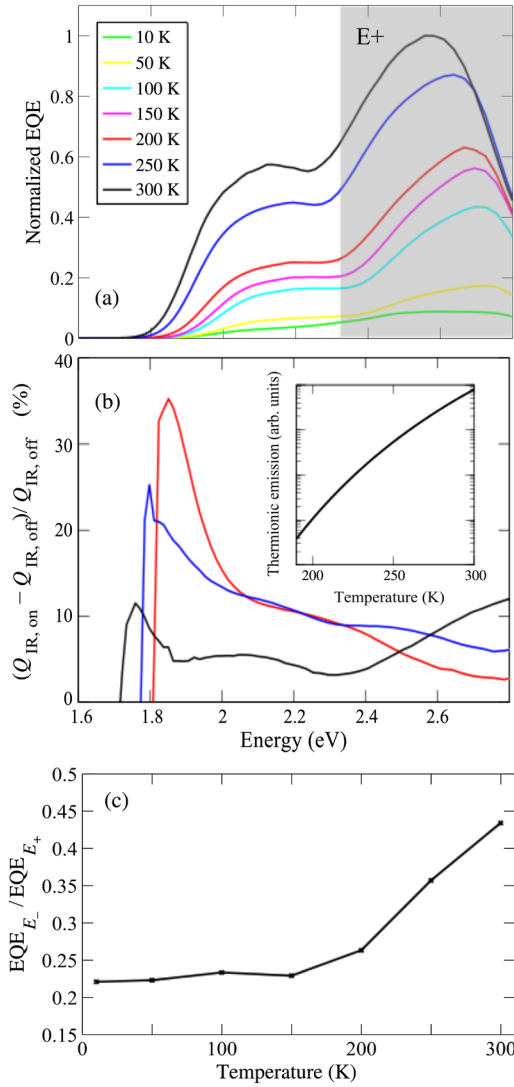


FIG. 5. Temperature-dependent behavior of (a) the EQE and (b) the increase in quantum efficiency with IR light of the sample SC1. The inset of (b) shows the thermionic emission rate over the AIP blocking layer as a function of temperature. (c) The ratio between the integrated EQE of the energy range corresponding to the  $E_-$  and the  $E_+$  energy transition [i.e., the shaded region of (a)].

is the most obvious indication of two-photon absorption. On the other hand, the decrease in EQE also at the high energies with the decreasing temperature is expected because the electrons that recombine from the  $E_+$  band to the  $E_-$  band are not able to escape to the  $n$ -GaP layer. However, the decrease in the temperature increases the lifetime of charge carriers, and therefore, will increase the relative magnitude of the EQE signal at the energy corresponding to the transition between the valence band and the  $E_+$  energy band [see Fig. 5(c)]. The observed saturation below 150 K, on the other hand, is most likely caused by the increased cell resistance at low temperatures.

### D. Impact of the $\text{GaAs}_{0.31}\text{P}_{0.68}\text{N}_{0.01}$ layer doping concentration

Experimental results show that the doping concentration inside the  $\text{GaAs}_{0.31}\text{P}_{0.68}\text{N}_{0.01}$  layer also affects the  $\Delta\text{QE}$  signal magnitude even if no blocking layer exists. Therefore, it is interesting to study the impact of the doping concentration of the  $\text{GaAs}_{0.31}\text{P}_{0.68}\text{N}_{0.01}$  layer on the photocurrent. Thus, we calculate the generation rates of various band-to-band transitions and generation-induced photocurrent as a function of the  $\text{GaAs}_{0.31}\text{P}_{0.68}\text{N}_{0.01}$  layer's electron density (shown in Fig. 6). Generation from the  $E_-$  band to the  $E_+$  band depends on the occupation of the initial states in the  $E_-$  band, and therefore, in order for two-photon absorption processes to occur effectively, it is advantageous to introduce donor doping for the  $E_-$  band, as also suggested by the results shown in Fig. 3. This observation is consistent with Marti *et al.* who propose that the optimum case for two-photon excitation is when the IB is half filled [26].

The advantage that is gained by  $n$ -type doping is that it guarantees the existence of charge carriers in the  $E_-$  energy band. The carrier concentration in the  $E_-$  band increases with the increasing  $n$ -type doping. Therefore, due to increased carrier concentration in the  $E_-$  energy band, low-energy photons are more likely to absorb exciting charge carriers from the  $E_-$  energy band to the  $E_+$  energy band. This agrees with the experimental results shown in Fig. 3. On the other hand, extensive doping of the  $E_-$  band may decrease generation from the valence band to the  $E_-$  band due to the lack of unoccupied final states. However, due to the band-structure parameters of the  $\text{GaAs}_{0.31}\text{P}_{0.68}\text{N}_{0.01}$  material studied here, the generation rate from the valence band to the  $E_-$  band is not yet largely affected by the doping densities, as shown in Fig. 6.

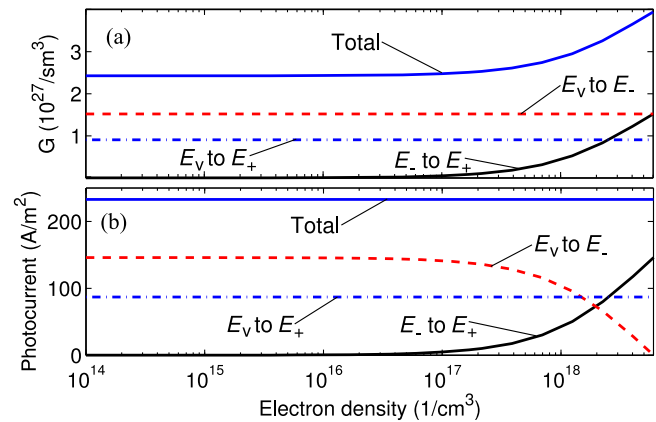


FIG. 6. (a) Total generation rates ( $G$ ) of different band-to-band transitions and (b) the photocurrent induced by the total generation rate as a function of  $n$ -type doping concentration in the  $\text{GaAs}_{0.31}\text{P}_{0.68}\text{N}_{0.01}$  layer.

### E. Current-voltage properties

Finally, we explain the impact on the  $I$ - $V$  properties of the experimental observations presented in this work. To perform this in the most straightforward way, the  $I$ - $V$  curves of  $\text{GaAs}_{0.31}\text{P}_{0.68}\text{N}_{0.01}$  solar cells are simulated under 1 Sun illumination and under the following operational premise. The simulated  $I$ - $V$  curves are shown in Fig. 7. First, we focus on two simulations S1 and S2, plotted with the dotted lines which show the artificial optimum and unfavorable cases, respectively, to draw the borders for the ideally operating  $\text{GaAs}_{0.31}\text{P}_{0.68}\text{N}_{0.01}$  IBSC. These borders should not be affected by current limitations in the quantitative understanding of the optical processes between the  $E_+$  and  $E_-$  bands. Note that S1 is calculated to prevent the recombination from the  $E_+$  energy band to the  $E_-$  energy band, blocking the current between the  $E_-$  energy band and the surrounding regions and not accounting for the recombination via the  $E_-$  band. Thereby, the curve S1 shows the optimum limit of the operation. On the other hand, the simulation S2 shows the device operation so that recombination is infinitely fast between the  $E_+$  and  $E_-$  energy bands and the current is not limited between the  $E_-$  energy band and the surrounding regions. Thus, in this case, all the electrons generated from the valence band to the  $E_+$  band are recombined to the  $E_-$  band before exiting the  $\text{GaAs}_{0.31}\text{P}_{0.68}\text{N}_{0.01}$  layer, and the photocurrent can flow freely between GaP and the  $E_-$  band of  $\text{GaAs}_{0.31}\text{P}_{0.68}\text{N}_{0.01}$ . As shown in Fig. 7, this unfavorable condition results in the

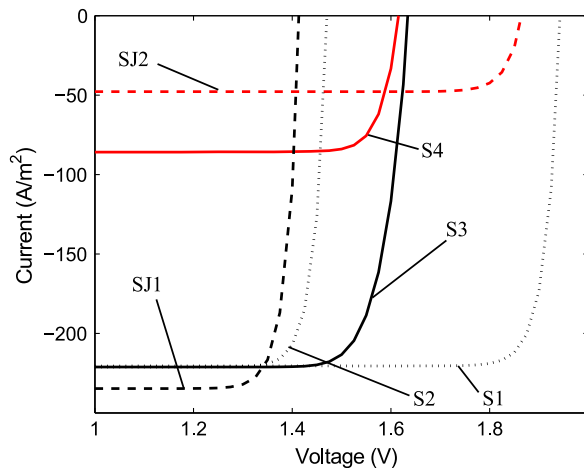


FIG. 7. Simulated  $I$ - $V$  curves of the six limiting cases of solar cell operation. Dotted curves show the  $I$ - $V$  curves so that all the photogenerated electrons from the valence band end up either in  $E_-$  or  $E_+$ , from which they can escape freely to the buffer layers. The open-circuit voltage is determined mainly by the radiative recombination rate, which exceeds the generation rate roughly at voltages corresponding to the  $E_-$  or the  $E_+$  band gap. Solid curves illustrate the effect of  $n$ -type doping to  $I$ - $V$  curves by accounting all the generation and recombination processes in the model. Dashed curves show the single-junction limits of the device with corresponding band gaps.

smaller open-circuit voltage. Therefore, as discussed in Ref. [8], in order to obtain maximum open-circuit voltage from  $\text{GaAs}_{1-x-y}\text{P}_y\text{N}_x$ -based solar cells, it is extremely important to block the current between the  $E_-$  energy band of  $\text{GaAs}_{1-x-y}\text{P}_y\text{N}_x$  and the conduction band of the device. As explained earlier, the observation of two-photon absorption is therefore promising as it implies the presence of an intermediate-band blocking layer. Furthermore, thermionic emission through the AIP barrier is an effect unfavorable for the optimum operation of an IBSC. Nonetheless, the observed traces of thermionic emission in temperature-dependent measurements provide additional evidence of IB blocking because thermionic emission is a leakage mechanism present in the case of intermediate-band solar cells.

Moreover, based on simulations S1 and S2, the  $\text{GaAs}_{1-x-y}\text{P}_y\text{N}_x$  layer should also be organized so that generation is efficient both between the  $E_-$  band and the valence band and between the  $E_+$  and  $E_-$  bands. Simulations S3 and S4 account for all the generation and recombination processes and are performed with the full model summarized in Sec. II to illustrate qualitatively how doping of the intermediate band affects the operation of the  $\text{GaAs}_{1-x-y}\text{P}_y\text{N}_x$  IBSC. We note that the impact of doping concentration in IB material is important information because the lifetimes of dilute nitrides are typically extremely short, as also observed in this work. As is explained in Sec. II, no current still flows between the  $E_-$  band and the surrounding regions, as in similar drift-diffusion simulations reported elsewhere [14–16]. The solid curves S3 and S4 in Fig. 7 show the simulated  $I$ - $V$  curves of the  $\text{GaAs}_{0.31}\text{P}_{0.68}\text{N}_{0.01}$ -based solar cell with different doping concentrations inside the  $\text{GaAs}_{0.31}\text{P}_{0.68}\text{N}_{0.01}$  layer. Note that simulation S3 is performed with the parameters of sample SC1, but to achieve a large generation from the  $E_-$  band to the  $E_+$  band, the  $n$ -type doping in  $\text{GaAs}_{0.31}\text{P}_{0.68}\text{N}_{0.01}$  is  $10^{19} \text{ cm}^{-3}$ . In simulation S4, the  $\text{GaAs}_{0.31}\text{P}_{0.68}\text{N}_{0.01}$  layer is undoped.

It can be observed that calculating the recombination between the  $E_+$  and  $E_-$  bands from their Fermi levels reduces the open-circuit voltage of the solar cell as compared to the ideal case S1. However, the black curve S3 has short-circuit current similar to simulations S1 and S2 due to doping the  $E_-$  band, which enables very efficient generation between the  $E_-$  and  $E_+$  bands. On the other hand, due to the lack of  $n$ -type doping concentration used in the red curve S4, the short-circuit current is smaller than that in simulations S1, S2, and S3, because the electron concentration in  $E_-$  is not sufficient for efficient two-photon absorption. As the current between the  $E_-$  energy band and the surrounding regions is blocked in simulation S4, almost all electrons generated to the  $E_-$  band return to the valence band by recombination. We note that a similar feature is also observed in Fig. 6, which shows that, by increasing the  $n$ -type doping concentration of

$\text{GaAs}_{0.31}\text{P}_{0.68}\text{N}_{0.01}$ , the magnitude of photocurrent in the  $E_+$  energy band increases. As a result, in order to optimize the operation of the  $\text{GaAs}_{1-x-y}\text{P}_y\text{N}_x$ -based IBSC, it is required that the recombination from the  $E_-$  band is much slower than the generation from the  $E_-$  band to the  $E_+$  band.

The advantages gained by blocking the IB can be briefly seen by comparing curves S1, S2, S3, and S4 to the dashed curves SJ1 and SJ2 in Fig. 7. Curves SJ1 and SJ2 show the limiting  $\text{GaAs}_{1-x}\text{P}_x$ -based single-junction simulations. The composition of the  $\text{GaAs}_{1-x}\text{P}_x$  materials in simulations is chosen so that their band-gap value matches as closely as possible either the transition-energy value between the  $E_-$  band and the valence band or the transition-energy value between the  $E_+$  band and the valence band in  $\text{GaAs}_{0.31}\text{P}_{0.68}\text{N}_{0.01}$ . The open-circuit voltages of simulations S1 and S2 are close to the corresponding simulations for the ideal and unfavorable cases of an intermediate-band solar cell due to similar turn-on voltage for recombination, and the small differences resulting from slightly different band-structure properties. Comparing simulation S3 to the single-junction simulation SJ1, it can be seen that both the inclusion of the two bands and an optimum generation between the  $E_-$  and  $E_+$  bands can significantly improve the performance of the solar cell at high voltages and power densities. The maximum power density from simulation S3 is  $320 \text{ W/m}^2$  and even from the unoptimal doping concentration of simulation S4, it is  $126 \text{ W/m}^2$ . Compared to the single-junction limits of simulation SJ1 and SJ2, where the power densities are  $302$  and  $82 \text{ W/m}^2$ , respectively, the  $\text{GaAs}_{0.31}\text{P}_{0.68}\text{N}_{0.01}$  fabricated here could ideally provide an enhancement of roughly 6% in power density, compared to corresponding  $\text{GaAs}_{1-x}\text{P}_x$ -based single-junction solar cells with the currently available material parameters and the layer and material structures considered in the simulations.

Last, we note that it has been predicted that, by optimization of the location of the energy bands of  $\text{GaAs}_{1-x-y}\text{P}_y\text{N}_x$  to cover the solar spectrum, the efficiency of the solar cell can increase in theory as high as 60% [7]. However, as discussed in this work, the open-circuit (OC) voltage of a solar cell  $V_{\text{OC}}$  cannot significantly exceed the effective band gap of the absorbing material that provides the photocurrent because of (1) the inverse process of recombination becoming stronger in the absorbing material and (2) diode leakage current increasing through the absorbing material to the barrier layers. Therefore, to obtain the maximum possible  $V_{\text{OC}}$  and, as a result, maximum conversion efficiency, the effective band gap of  $\text{GaAs}_{1-x-y}\text{P}_y\text{N}_x$  should be the  $E_+$  energy band. Then, the voltage of the solar cell could be determined by the difference of the valence band and the  $E_+$  band quasi-Fermi-levels. In thermionic emission theory, electron systems on different sides of a potential barrier have different quasi-Fermi-levels and the current between them is

exponentially dependent on the height of the potential barrier. Thus, a suitably chosen potential barrier material, like AIP, must be implemented in the heterostructure. We also note that the effect of AIP blocking layer can be enlarged if the arsenic or nitrogen content of  $\text{GaAs}_{1-x-y}\text{P}_y\text{N}_x$  is increased. The next step for  $\text{GaAs}_{1-x-y}\text{P}_y\text{N}_x$  IBSCs seems to be to demonstrate the increase in open-circuit voltage experimentally and to show that the electron system in the  $E_-$  band is separated from the electrons in the buffer layer. Furthermore, comparative simulations also indicate that careful band engineering of the blocking layers next to the  $\text{GaAs}_{1-x-y}\text{P}_y\text{N}_x$  layer is expected to further block the leakage current of the diode and enable larger  $V_{\text{OC}}$  and higher fill factors, due to the improved use of photogeneration between the  $E_-$  and  $E_+$  bands at voltages close to  $V_{\text{OC}}$ . Therefore, the most important considerations in the development of the  $\text{GaAs}_{1-x-y}\text{P}_y\text{N}_x$ -based IBSC seem to be (i) optimizing the bands so that recombination from the  $E_-$  band to the valence band is suppressed and the electrons in the  $E_-$  band are excited to the  $E_+$  band and (ii) blocking the current through the  $E_-$  band so that it does not act as a leakage or recombination path.

#### IV. CONCLUSIONS

The experimental results, measured from a solar cell in which a  $\text{GaAs}_{0.31}\text{P}_{0.68}\text{N}_{0.01}$  layer is implemented in the heterostructure and isolated using an AIP blocking layer, show that two-photon absorption can occur in the  $\text{GaAs}_{0.31}\text{P}_{0.68}\text{N}_{0.01}$  solar cell. The absorption of IR light with photon energy smaller than the transition between the valence band and the  $E_-$  band increased the quantum efficiency by over 10% at room temperature and more at lower temperatures due to the suppression in the thermionic emission. The observed transition energies in the EQE spectrum correspond to the  $E_-$  and  $E_+$  energy bands of the  $\text{GaAs}_{0.31}\text{P}_{0.68}\text{N}_{0.01}$  alloy and agree with the photoreflectance results. Device simulations are used to study the effects of two-photon absorption on the  $I$ - $V$  characteristics and output power of the fabricated  $\text{GaAs}_{0.31}\text{P}_{0.68}\text{N}_{0.01}$  solar cell. We consider four relevant limiting cases of the ideally operating  $\text{GaAs}_{0.31}\text{P}_{0.68}\text{N}_{0.01}$  IBSC and two  $\text{GaAs}_{1-x}\text{P}_x$ -based reference solar cells in terms of current transport and optical transitions. We also discuss the potential benefits of  $\text{GaAs}_{1-x-y}\text{P}_y\text{N}_x$  in terms of higher peak efficiencies and output powers, as well as ways to achieve them based on (i) achieving favorable generation-recombination properties in the band structure of  $\text{GaAs}_{1-x-y}\text{P}_y\text{N}_x$  and (ii) suppressing current between  $E_-$  and the surrounding regions using suitable potential barriers. Satisfying these conditions will enable harvesting a large part of the solar spectrum, determining  $V_{\text{OC}}$  by  $E_+$ , and achieving very high efficiencies compared to conventional single-junction solar cells.

## ACKNOWLEDGMENTS

We acknowledge the provision of facilities and technical support by Aalto University at Micronova Nanofabrication Centre. This work was in part supported by the Academy of Finland, the Graduate School of Modern Optics and Photonics, the Ulla Tuominen Foundation, and the Nokia Foundation.

- 
- [1] A. Luque and A. Martí, Increasing the Efficiency of Ideal Solar Cells by Photon Induced Transitions at Intermediate Levels, *Phys. Rev. Lett.* **78**, 5014 (1997).
- [2] A. Luque, A. Martí, and C. Stanley, Understanding intermediate-band solar cells, *Nat. Photonics* **6**, 146 (2012).
- [3] A. Martí, E. Antolin, E. Canovas, N. Lopez, P. G. Linares, A. Luque, C. R. Stanley, and C. D. Farmer, Elements of the design and analysis of quantum-dot intermediate band solar cells, *Thin Solid Films* **516**, 6716 (2008).
- [4] E. Antolin, A. Martí, C. R. Stanley, C. D. Farmer, E. Canovas, N. Lopez, P. G. Linares, and A. Luque, Low temperature characterization of the photocurrent produced by two-photon transitions in a quantum dot intermediate band solar cell, *Thin Solid Films* **516**, 6919 (2008).
- [5] S. Asahi, H. Teranishi, N. Kasamatsu, T. Kada, T. Kaizu, and T. Kita, Suppression of thermal carrier escape and efficient photo-carrier generation by two-step photon absorption in InAs quantum dot intermediate-band solar cells using a dot-in-well structure, *J. Appl. Phys.* **116**, 063510 (2014).
- [6] J. Hwang, K. Lee, A. Teran, S. Forrest, J. D. Phillips, A. J. Martin, and J. Millunchick, Multiphoton Sub-Band-Gap Photoconductivity and Critical Transition Temperature in Type-II GaSb Quantum-Dot Intermediate-Band Solar Cells, *Phys. Rev. Applied* **1**, 051003 (2014).
- [7] K. M. Yu, W. Walukiewicz, J. W. Ager, D. Bour, R. Farshchi, O. D. Dubon, S. X. Li, I. D. Sharp, and E. E. Haller, Multiband GaNAsP quaternary alloys, *Appl. Phys. Lett.* **88**, 092110 (2006).
- [8] N. López, L. A. Reichertz, K. M. Yu, K. Campman, and W. Walukiewicz, Engineering the Electronic Band Structure for Multiband Solar Cells, *Phys. Rev. Lett.* **106**, 028701 (2011).
- [9] N. Ahsan, N. Miyashita, M. M. Islam, K. M. Yu, W. Walukiewicz, and Y. Okada, Two-photon excitation in an intermediate band solar cell structure., *Appl. Phys. Lett.* **100**, 172111 (2012).
- [10] T. Tanaka, M. Miyabara, Y. Nagao, K. Saito, Q. Guo, M. Nishio, K. M. Yu, and W. Walukiewicz, Photogenerated current by two-step photon excitation in ZnTeO intermediate band solar cells with n-ZnO window layer., *IEEE J. Photovoltaics* **4**, 196 (2014).
- [11] A. Luque and A. Martí, Photovoltaics: Towards the intermediate band, *Nat. Photonics* **5**, 137 (2011).
- [12] R. Kudrawiec, A. V. Luce, M. Gladysiewicz, M. Ting, Y. J. Kuang, C. W. Tu, O. D. Dubon, K. M. Yu, and W. Walukiewicz, Electronic Band Structure of GaNPAs Highly Mismatched Alloys: Suitability for Intermediate-Band Solar Cells, *Phys. Rev. Applied* **1**, 034007 (2014).
- [13] J-M. Tilli, H. Jussila, K. M. Yu, T. Huhtio, and M. Sopanen, Composition determination of quaternary GaAsPN layers from single x-ray diffraction measurement of quasi-forbidden (002) reflection, *J. Appl. Phys.* **115**, 203102 (2014).
- [14] K. Yoshida, Y. Okada, and N. Sano, Self-consistent simulation of intermediate band solar cells: Effect of occupation rates on device characteristics, *Appl. Phys. Lett.* **97**, 133503 (2010).
- [15] A. S. Lin and J. D. Phillips, Drift-diffusion modeling for impurity photovoltaic devices, *IEEE Trans. Electron Devices* **56**, 3168 (2009).
- [16] T. Nozawa and Y. Arakawa, Theoretical analysis of multi-level intermediate-band solar cells using a drift diffusion model, *J. Appl. Phys.* **113**, 243102 (2013).
- [17] P. Kivisaari, J. Oksanen, and J. Tulkki, Effects of lateral current injection in GaN multi-quantum well light-emitting diodes, *J. Appl. Phys.* **111**, 103120 (2012).
- [18] H. A. Tahini, A. Chronos, S. T. Murphy, U. Schwingenschlogl, and R. W. Grimes, Vacancies and defect levels in III-V semiconductors, *J. Appl. Phys.* **114**, 063517 (2013).
- [19] I. Vurgaftman, J. R. Meyer, and L. R. Ram-Mohan, Band parameters for III-V compound semiconductors and their alloys, *J. Appl. Phys.* **89**, 5815 (2001).
- [20] M. Levinshtein, M. S. Shur, and S. Rumyanstev, *Ternary and Quaternary III-V Compounds*, Handbook Series on Semiconductor Parameters Vol. 2 (World Scientific, Singapore, 1996).
- [21] W. Shan, W. Walukiewicz, J. W. Ager, E. E. Haller, J. F. Geisz, D. J. Friedman, J. M. Olson, and S. R. Kurtz, Band Anticrossing in GaInNAs Alloys, *Phys. Rev. Lett.* **82**, 1221 (1999).
- [22] H. Jussila, K. M. Yu, J. Kujala, F. Tuomisto, S. Nagarajan, J. Lemettinen, T. Huhtio, T. O. Tuomi, H. Lipsanen, and M. Sopanen, Substitutionality of nitrogen atoms and formation of nitrogen complexes and point defects in GaPN alloys, *J. Phys. D* **47**, 075106 (2014).
- [23] D. B. Jackrel, S. R. Bank, H. B. Yuen, M. A. Wistey, J. S. Harris, A. J. Ptak, S. W. Johnston, D. J. Friedman, and S. R. Kurtz, Dilute nitride GaInNAs and GaInNAsSb solar cells by molecular beam epitaxy, *J. Appl. Phys.* **101**, 114916 (2007).
- [24] Y. J. Kuang, K. M. Yu, R. Kudrawiec, A. V. Luce, M. Ting, W. Walukiewicz, and C. W. Tu, GaNAsP: An intermediate band semiconductor grown by gas-source molecular beam epitaxy, *Appl. Phys. Lett.* **102**, 112105 (2013).
- [25] A. Schenk, A model for the field and temperature dependence of Shockley-Read-Hall lifetimes in silicon, *Solid State Electron.* **35**, 1585 (1992).
- [26] A. Luque and A. Martí, A metallic intermediate band high efficiency solar cell, *Prog. Photovoltaics* **9**, 73 (2001).